Hindawi
Shock and Vibration
Volume 2023, Article ID 6234753, 11 pages
https://doi.org/10.1155/2023/6234753

Research Article

Measurement Technique and Result Analysis of Helicopter Rotor Blade Structural Vibration Load

Honglin Zhang,[1,2] Zefeng Wang,[1] and Pinqi Xia[2]

[1]*Institute of Flight Test Technology, Chinese Flight Test Establishment, Xi'an 710089, China*
[2]*College of Aerospace Engineering, Nanjing University of Aeronautics and Astronautics, Nanjing 210016, China*

Correspondence should be addressed to Zefeng Wang; wangzijun567@163.com

Received 16 November 2022; Revised 12 April 2023; Accepted 16 May 2023; Published 2 June 2023

Academic Editor: Francesco Bucchi

The measurement of helicopter rotor blade structural load amid flight has always been the difficulty in flight test. In this paper, the principle of the existing blade structural load measurement method (electrical measurement method) was analyzed, and the problem of physical decoupling in the use of this method was expounded. As a weak signal measurement, the electrical measurement method also has electromagnetic interference problems, which will affect the flight test period of blade structural load measurement. Therefore, a numerical decoupling measurement method based on fiber Bragg grating (FBG) was proposed. Then, the new method was applied and verified in the load equation modeling test and the flight test under the real atmospheric environment was carried out. Through comparing and analyzing the measured data of the new method and the electrical measurement one, the correctness of the FBG data decoupling method was validated. The results indicate that the method proposed in this paper can effectively improve the efficiency of blade load equation modeling engineering and has good application value.

1. Introduction

In the course of flight, the helicopter obtains the required lift force and handling force through the rotor, specifically the movement of the blade. In the process of rotation, the blade is easily subjected to the action of periodic aerodynamic force, which undergoes flapwise motion, edgewise motion, and torsional motion. From the point of view of structural load, the blade bears the flapwise bending moment, edgewise bending moment, torque, and other multiaxis loads. The structural load level of the blade cross-section has been a concern in the design process, which determines the static strength and fatigue strength of the blade and reflects the aerodynamic design results of the rotor blade to a certain extent. Therefore, the measurement of the structural load of the rotor blade is always a necessary work in the course of a flight test.

The helicopter rotor structural load is currently measured based on the traditional electrical measurement method [1–5]. However, it, as a weak current signal measurement method, is susceptible to electromagnetic interference, which to a certain extent affects the flight test period of blade structural load measurement.

In this paper, the characteristics of helicopter rotor blade structural load measurement based on FBG technology [6, 7] were analyzed and investigated.

2. Analysis of Blade Structural Load Measurement Method

Figure 1 is the structural load diagram of the helicopter rotor blade cross-section, in which flapwise bending moment is perpendicular to the chord direction of the blade, edgewise bending moment is parallel to it, and α is the blade pitch angle relative to the hub plane. Torque is the resultant moment about the blade pitch axis, located at the quarter-chord point.

Figure 2 shows the principle of the blade structural load measurement by the traditional electrical measurement

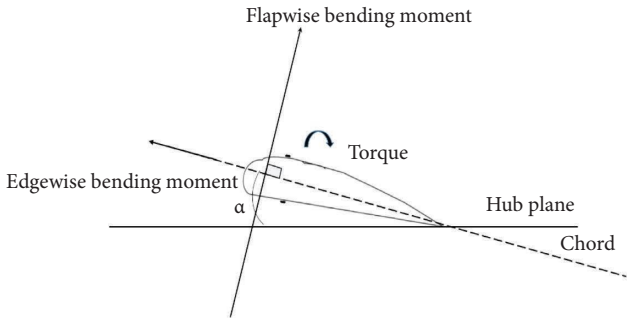

Figure 1: Schematic diagram of structural load of blade cross-section.

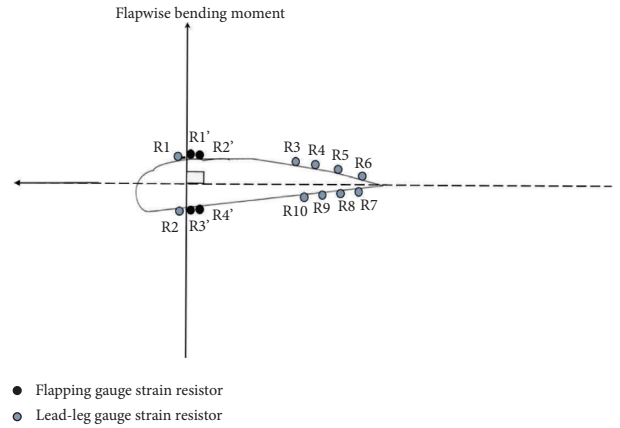

Figure 2: Principle of load measurement by the electrical method.

method. It is to install resistance strain gauges at the upper and lower surfaces of the blade, respectively. That is to say, 4 resistors, namely, R1′, R2′, R3′, and R4′ in Figure 2, were used to form a strain bridge for flapwise bending moment measurement; from the 10 resistors R1~R10, as shown in Figure 2, 4 resistors were selected to form a strain bridge, and the edgewise bending moment was measured. The selection principles is determined by the coupling coefficient of flapwise and edgewise strain bridges, which is usually no more than 5% among the engineering.

Electrical measurement method was proposed based on the physical decoupling idea of blade flapwise and edgewise loads [8]. When it is used to measure blade structural loads, in addition to the aforementioned weak current signal electromagnetic interference, there is also the work of repeated selection of the strain gauge, which affects the test progress to a certain extent.

What is more, due to the limitation of the fatigue life of the electric strain gauge, in the use of the method, the flapwise bending moment bridge and edgewise bending moment bridge are prone to being damaged, which results in a failure to measure the blade flapwise structural load and edgewise structural load synchronously during the flight test period.

As the communication medium of the FBG sensor, optical fiber has good tensile and bending resistance [9–12], and good adaptability in the helicopter blade vibration environment. Therefore, it can be used to measure the blade structural loads by using the idea of numerical decoupling [13–15]. The measurement principle is shown in Figure 3. For the flapwise and edgewise bending moments measurement, along the blade pitch axis, two FBG sensors were arranged on the upper and lower surfaces of the blade, respectively; along the blade edgewise direction, two FBG sensors were assembled on the leading and trailing edges of the blade, respectively. For the torque measurement, on the upper and lower surfaces of the blade, two FBG sensors were installed at ±45 deg angles with the blade pitch axis, respectively.

In Figure 3, F_{up} and F_{down} represent the linear strains measured along the blade pitch axis, on the upper and lower surfaces of the blade, respectively. Lfront and Lback denote the linear strains measured on the leading and trailing edges of the blade, respectively. $\varphi_{\text{u+}}$ and $\varphi_{\text{u-}}$ refer to the strains for the torque measurement on the upper surface of the blade. $\varphi_{\text{d+}}$ and $\varphi_{\text{d-}}$ represent the strains for the torque measurement on the lower surface of the blade.

The linear strains F_{up} and F_{down} can be calculated by the following formulas:

$$F_{\text{up}} = F_{\text{up}}(F) + F_{\text{up}}(M_F) + F_{\text{up}}(M_L) + F_{\text{up}}(T), \tag{1}$$

$$F_{\text{down}} = F_{\text{down}}(F) + F_{\text{down}}(M_F) + F_{\text{down}}(M_L) + F_{\text{down}}(T), \tag{2}$$

where F, M_F, M_L, and T represent the centrifugal force, flapwise bending moment, edgeswise bending moment, and torque of the blade cross-section, respectively.

For strain components on the right-hand sides of equations (1) and (2), there are the following formulas:

$$\begin{aligned} F_{\text{up}}(F) &= F_{\text{down}}(F), \\ F_{\text{up}}(T) &= F_{\text{down}}(T). \end{aligned} \tag{3}$$

It can be obtained from equations (1) and (2) that

$$\begin{aligned} \Delta F = F_{\text{up}} - F_{\text{down}} &= F_{\text{up}}(M_F) + F_{\text{up}}(M_L) \\ &- F_{\text{down}}(M_F) - F_{\text{down}}(M_L). \end{aligned} \tag{4}$$

That is to say, along the blade pitch axis, the linear strain difference between the upper and lower surfaces of the blade is a binary function of flapwise bending moment and edgewise bending moment.

Similarly, the linear strain difference between the leading and trailing edges of the blade is a binary function of the edgewise bending moment and flapwise bending moment. Then, for ΔF and ΔL, there is the following relation:

$$\begin{bmatrix} \Delta F \\ \Delta L \end{bmatrix} = \begin{bmatrix} b_{11} & b_{12} \\ b_{21} & b_{22} \end{bmatrix} \begin{bmatrix} M_F \\ M_L \end{bmatrix}. \tag{5}$$

For the strains of the torque measurement on the upper surface of the blade, there is

$$\phi_{u+} = \phi_{u+}(F) + \phi_{u+}(M_F) + \phi_{u+}(M_L) + \phi_{u+}(T), \tag{6}$$

$$\phi_{u-} = \phi_{u-}(F) + \phi_{u-}(M_F) + \phi_{u-}(M_L) + \phi_{u-}(T). \tag{7}$$

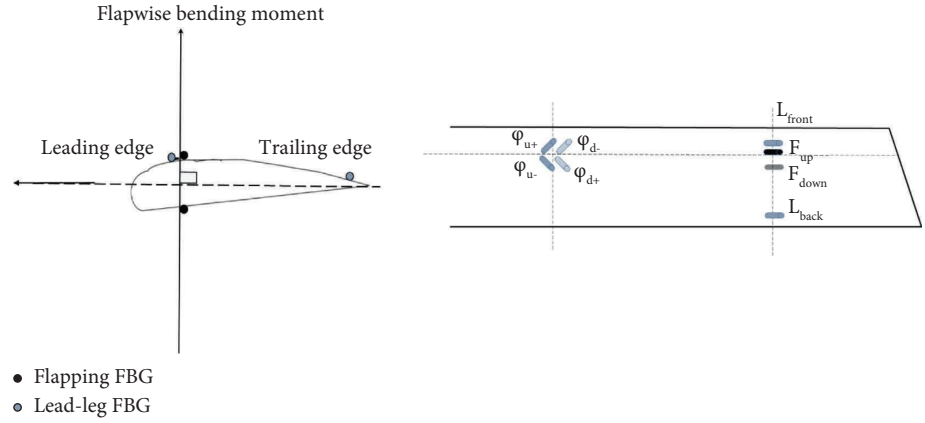

Figure 3: Load measurement principle of FBG method.

Table 1: Description of blade load measurement.

Section 1	Section 2	Section 3	Section 4	Section 5	Section 6	Section 7
0.01R	0.05R	0.20R	0.36R	0.44R	0.54R	0.67R
Flapwise bending moment	Torsion moment	Flapwise bending moment	Flapwise bending moment	Flapwise bending moment	Flapwise bending moment	Flapwise bending moment
Edgewise bending moment	—	Edgewise bending moment	Edgewise bending moment	Edgewise bending moment	Edgewise bending moment	Edgewise bending moment

It can be drawn from equations (6) and (7) that the strain components are caused by the centrifugal force, flapwise bending moment, edgewise bending moment, and torque, respectively. For these strain components, the following relations exist:

$$\begin{aligned} \phi_{u+}(F) &= \phi_{u-}(F), \\ \phi_{u+}(M_F) &= \phi_{u-}(M_F), \\ \phi_{u+}(M_L) &= \phi_{u-}(M_L). \end{aligned} \tag{8}$$

It can be obtained from equations (6) and (7) that

$$\Delta\phi = \phi_{u+} - \phi_{u-} = \phi_{u+}(T) - \phi_{u-}(T). \tag{9}$$

Evidently, $\Delta\phi$, the strain difference of the two FBG sensors for the torque measurement on the upper surface of the blade is a linear function of the cross-section torque. For the lower surface, the same conclusion is reached. Hence, the following formula can be obtained

$$\Delta\phi = B \times T. \tag{10}$$

Based on the above analysis, the principle of multiaxis numerical decoupling can be used to measure the blade structural loads by FBG method.

3. Load Equation Modeling

The blades were instrumented with 28 FBG sensors to measure structural loads at seven radial stations, as shown in Table 1. Flapwise, edgewise, and torsion moments were measured at 6, 6, and 1 radial stations, respectively.

The corresponding load data were obtained through static loading tests on the ground. The loading conditions contain a pure flapwise bending moment, a pure edgewise bending moment, a combined flapwise-edgewise bending moment, and pure torsion moment. The represented results of these tests are shown in Figures 4–7.

It can be seen from Figure 4 that the flapping and torsion output responses of section 1 were basically unchanged when it was loaded in the edgewise direction. As can be seen from Figure 5, when section 1 was loaded in the flapwise direction, the output response of torsion was roughly unchanged, while the output response of lag varied within a small range. According to Figure 6, the output responses of flapping and torsion of section 2 remained basically unchanged when the load was applied in the edgewise direction. Likewise, as can be seen from Figure 7, when section 2 was loaded in a flapwise direction, the output response of torsion kept basically unchanged, while the output responses of flapping and lag presented a linear variation. The above phenomena verify the correctness of the measurement principle of the FBG method.

The load comparison curves of sections 1 and 3 are shown in Figures 8 and 9. It can be seen that the estimated and measured flapwise and edgewise bending moments have the same variation trend for both sections.

Tables 2 and 3 show the error analysis of the bending moments of sections 1 and 3. It can be seen that the maximum error of the flapwise bending moment of section 1 was 1.3%, while that of the edgewise bending moment was 5.1%. For section 3, the maximum error of the flapwise bending moment was 2.7% and that of the edgewise bending moment was 4.9%, which meets the engineering requirements.

Figure 10 shows the comparison of estimated and measured torques of section 2. It can be seen that the

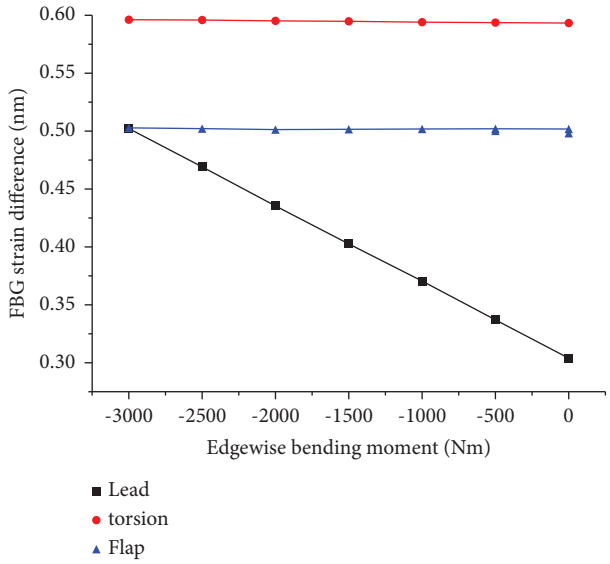

Figure 4: Calibration test curve of section 1 under edgewise direction loading condition.

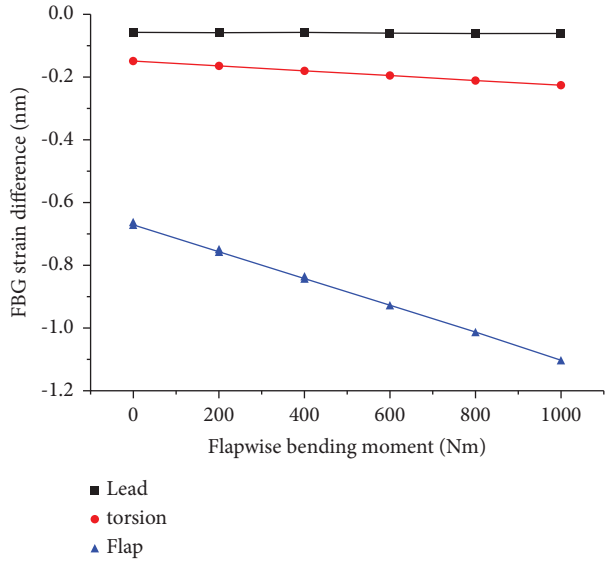

Figure 5: Calibration test curve of section 1 under flapwise direction loading condition.

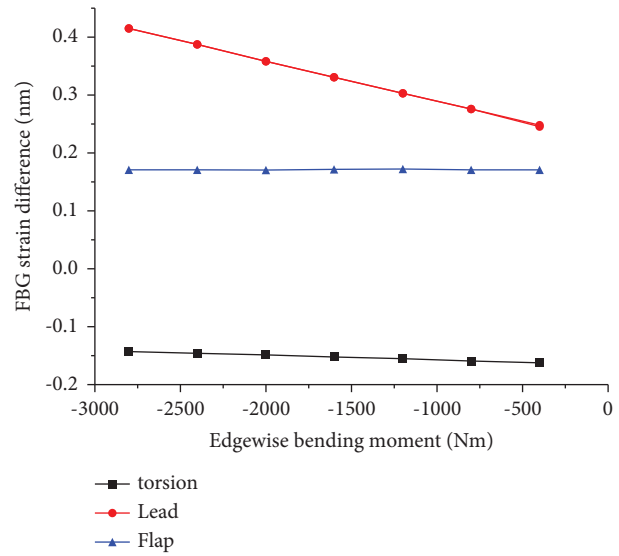

Figure 6: Calibration test curve of section 3 under edgewise direction loading condition.

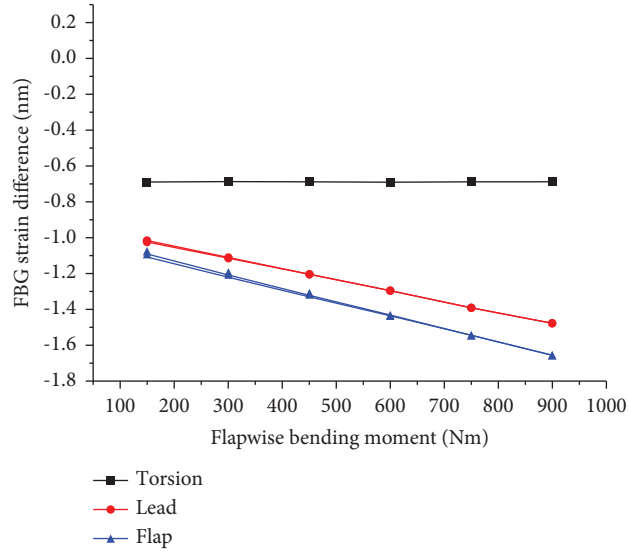

Figure 7: Calibration test curve of section 3 under flapwise direction loading condition.

estimated torque was basically consistent with the measured value. Table 4 shows the corresponding error analysis. The maximum error between the estimated value and the measured one was 4.3%, satisfying the engineering requirements.

4. Analysis of Flight Test Results

The test equipment installation is shown in Figure 11. Typical hover and forward flight conditions were selected for flight test measurement. Blade structural load Figure 12 obtained by the FBG method Figure 13 are compared with Figure 14 those obtained by electric Figure 15 measurement method. The results for two blade cross-sections at radial stations of 0.20R and 0.40R under two different advance ratios ($\mu = 0.20$ and $\mu = 0.23$) are shown in Figures 12–16.

It can be seen from Figures 12–16 that blade structural loads have almost the same variation trends for the two measurement methods. This indicates that the FBG sensor shows good following performance for the blade structural dynamic load measurement. It should be noted that the maximum or minimum values of the blade structural loads are also captured by the FBG method, which are important for fatigue characteristic analysis of the blade.

The difference, mainly reflected in the load magnitude, may be caused by the takeoff weight or the air density.

Furthermore, the blade structural loads obtained by the FBG method were analyzed in the frequency domain.

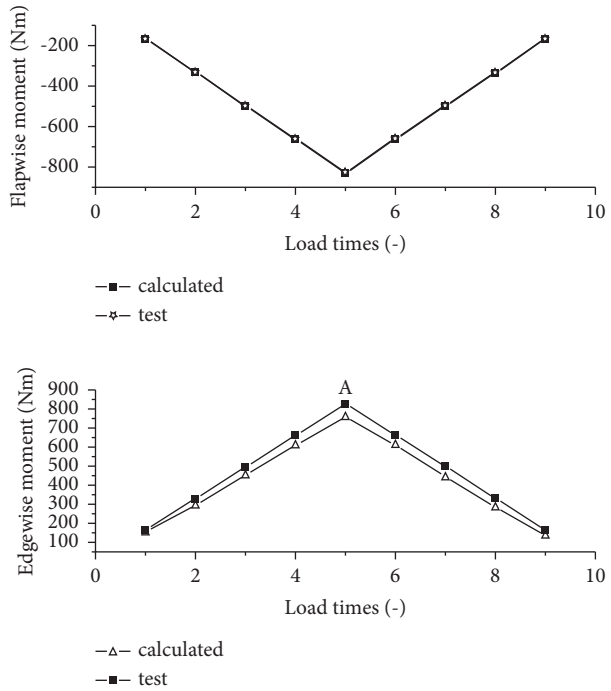

Figure 8: Comparison of calculated and measured flapwise and edgewise bending moments of section 1.

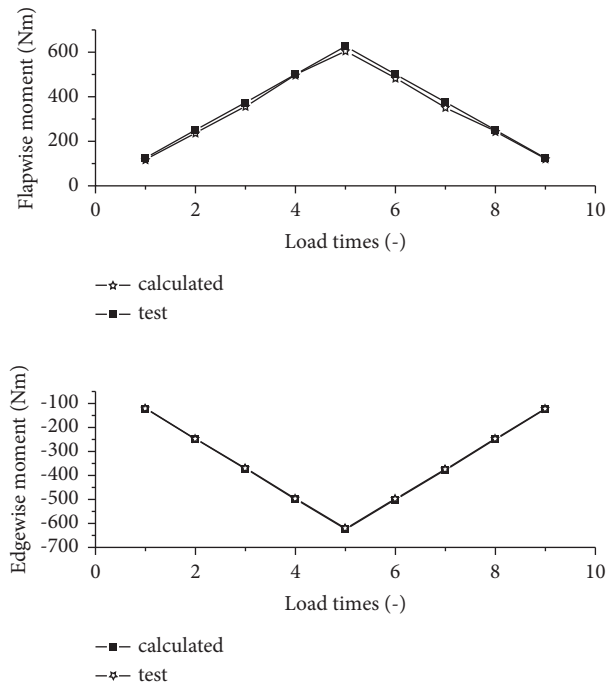

Figure 9: Comparison of calculated and measured flapwise and edgewise bending moments of section 3.

Table 2: Load comparison data of section 1.

Flapwise moment test value (Nm)	Flapwise moment calculated value (Nm)	Error	Edgewise moment test value (Nm)	Edgewise moment calculated value	Error
−165.801	−167.969	0.013	165.801	157.501	−0.050
−331.602	−335.938	0.013	331.602	316.314	−0.046
−496.496	−501.153	0.009	496.496	482.815	−0.028
−661.951	−666.368	0.007	661.951	630.315	−0.048
−827.061	−828.830	0.002	827.061	797.972	−0.035
−661.951	−663.615	0.003	661.951	629.315	−0.049
−496.496	−498.400	0.004	496.496	470.971	−0.051
−331.602	−333.184	0.005	331.602	315.470	−0.049
−165.801	−167.969	0.013	165.801	158.813	−0.042

Table 3: Load comparison data of section 3.

Flapwise moment test value (Nm)	Flapwise moment calculated value (Nm)	Error	Edgewise moment test value (Nm)	Edgewise moment calculated value	Error
−125.381	−121.970	−0.027	125.381	119.964	−0.043
−250.762	−247.028	−0.015	250.762	237.075	−0.045
−375.457	−368.998	−0.017	375.457	357.186	−0.049
−500.577	−495.600	−0.010	500.577	497.019	−0.007
−625.436	−619.114	−0.010	625.436	607.409	−0.029
−500.577	−498.688	−0.004	500.577	485.724	−0.030
−375.457	−373.630	−0.005	375.457	352.466	−0.041
−250.762	−247.028	−0.015	250.762	245.222	−0.022
−125.381	−123.514	−0.015	125.381	120.390	−0.040

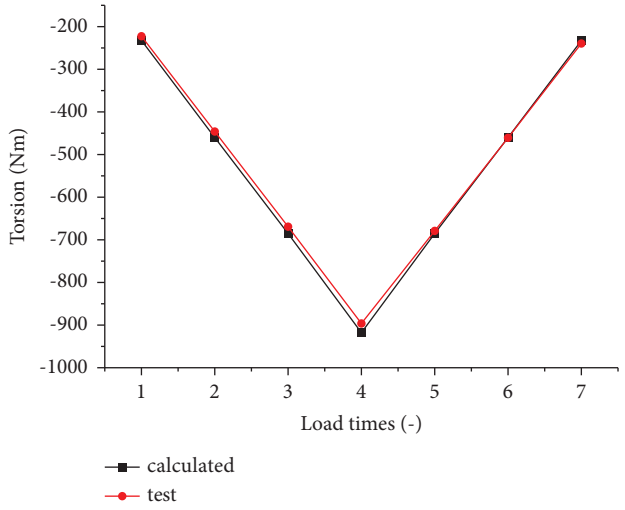

Figure 10: Comparison of calculated and measured torque of section 2.

Table 4: Load comparison data of section 2.

Actual torque value (Nm)	Calculated torque value (Nm)	Error
−232.296	−222.325	−0.043
−459.812	−446.195	−0.030
−686.120	−670.064	−0.023
−918.370	−897.021	−0.023
−686.120	−679.327	−0.010
−459.812	−461.634	0.004
−232.296	−239.309	0.030

Figure 11: Installation of test equipment.

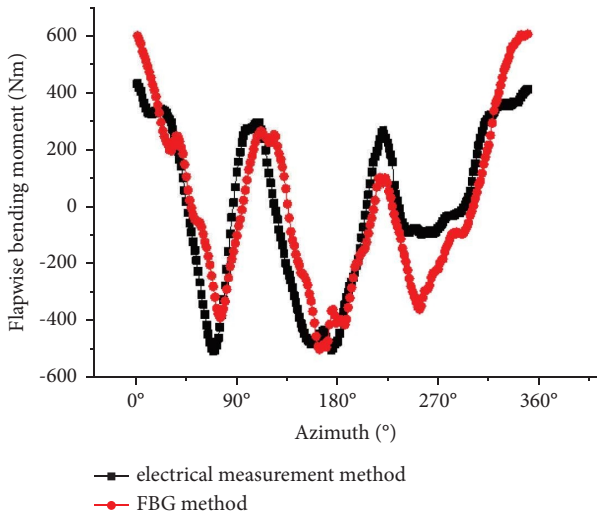

Figure 12: Comparison of flapwise bending moment for blade cross-section at 0.20R ($\mu = 0.20$).

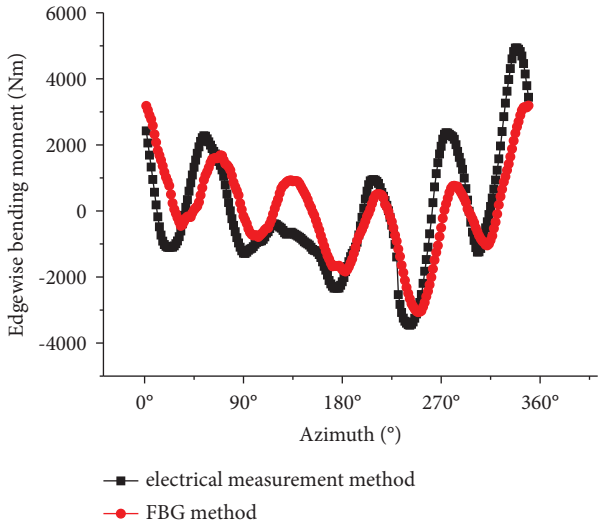

Figure 13: Comparison of egdewise bending moment for blade cross-section at 0.20R ($\mu = 0.20$).

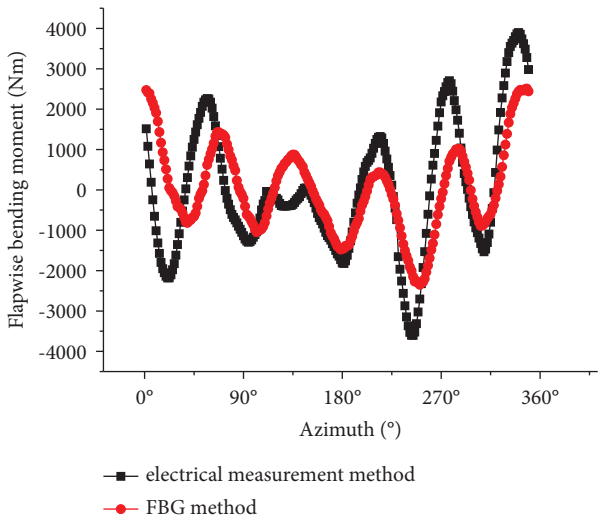

Figure 14: Comparison of flapwise bending moment for blade cross-section at 0.44R ($\mu = 0.20$).

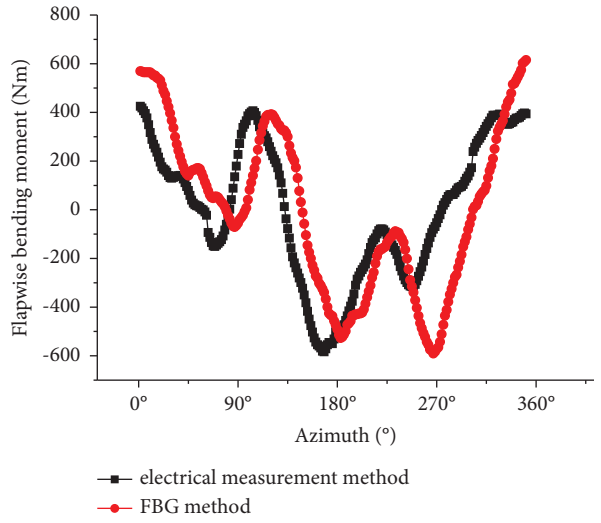

Figure 15: Comparison of flapwise bending moment for blade cross-section at 0.20R ($\mu = 0.23$).

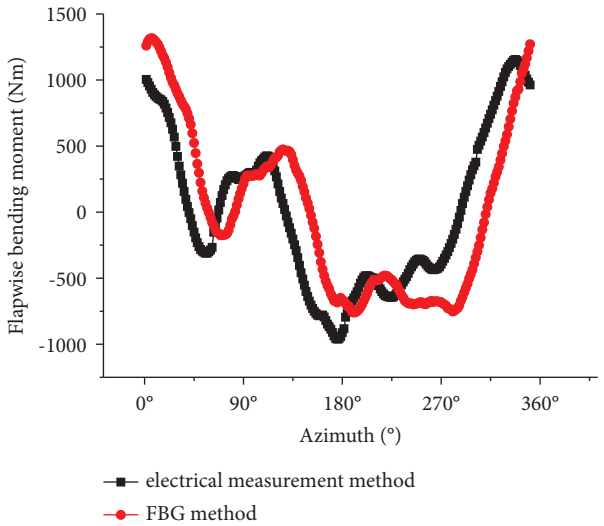

Figure 16: Comparison of flapwise bending moment for blade cross-section at 0.44R ($\mu = 0.23$).

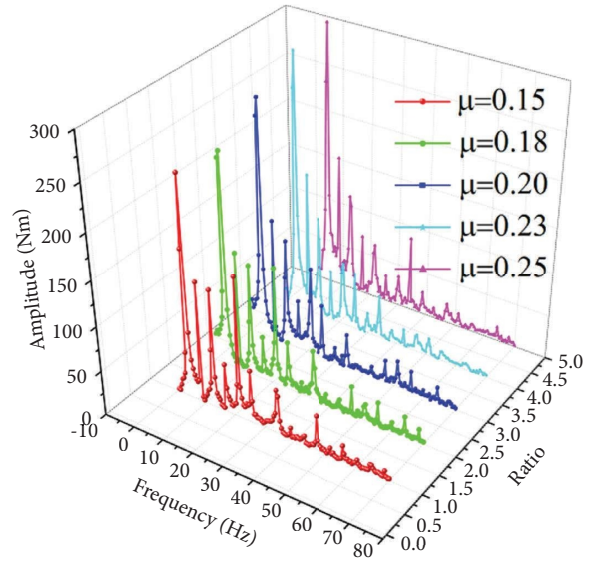

Figure 17: The variations of the harmonic coefficients of blade flapwise bending moment with advance ratios at radial station of 0.01R.

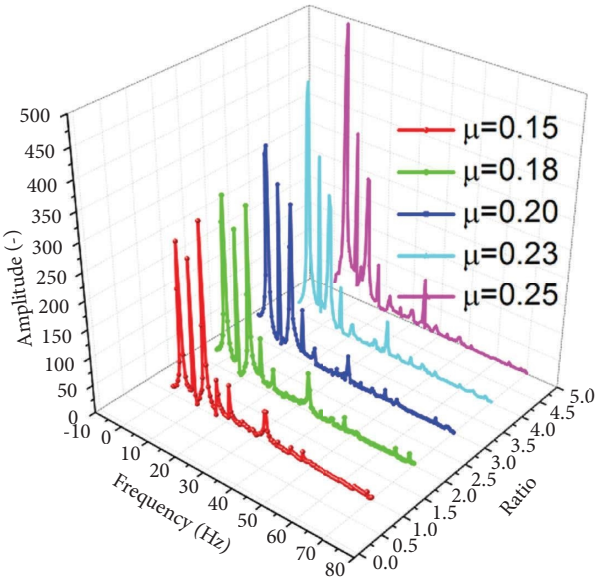

Figure 18: The variations of the harmonic coefficients of blade flapwise bending moment with advance ratios at radial station of 0.36R.

Figures 17–19 show the variations Figure 18 of the harmonic coefficients of blade Figure 19 flapwise bending moment with advance ratios at radial stations of 0.01R, 0.36R, and 0.67R, respectively.

It is evident that the first three harmonic coefficients are dominant, which correctly reflects the typical characteristic of blade vibration.

Figure 20 shows the variations of the harmonic coefficients of blade flapwise bending moment with radial stations at advance ratio of 0.23.

For the same harmonic coefficient, its value generally increases as the radial position of the blade increases.

In summary, the blade structural loads obtained by FBG numerical analysis method were compared in time domain

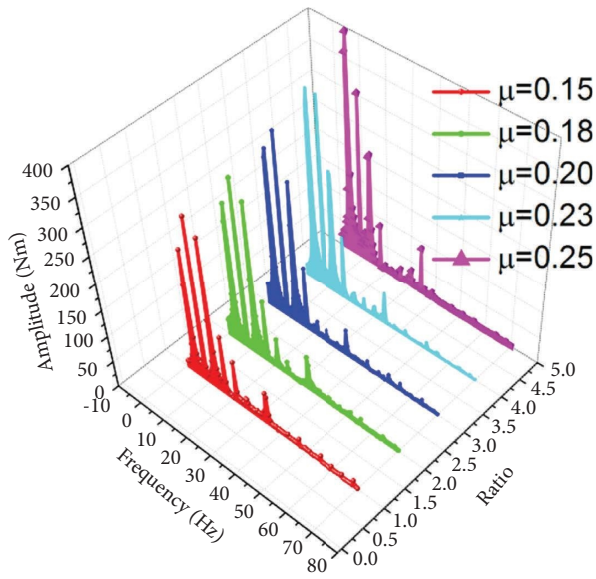

Figure 19: The variations of the harmonic coefficients of blade flapwise bending moment with advance ratios at radial station of 0.67R.

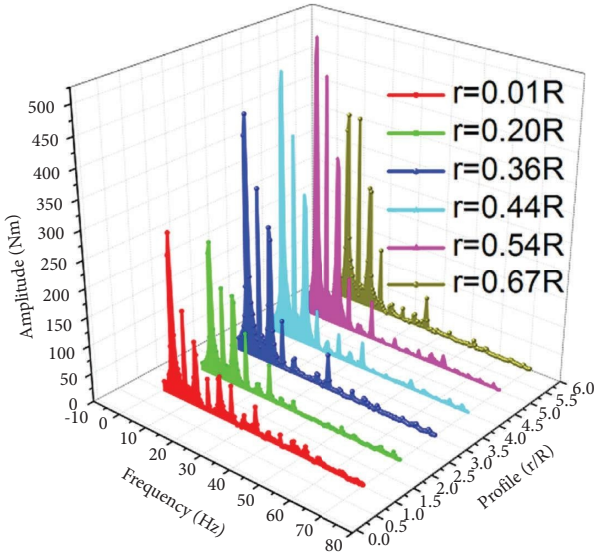

Figure 20: The variations of the harmonic coefficients of blade flapwise bending moment with radial stations ($\mu = 0.23$).

and frequency domain, and the feasibility of the method was validated.

5. Conclusion

Through aforementioned research, the following conclusions are drawn as follows:

(1) In view of the problems arose by the traditional electrical measurement method, a new numerical decoupling method based on FBG sensor was proposed to measure the blade structural loads

(2) The correctness and feasibility of the new method are verified by load equation modeling test and flight test

(3) The method proposed in this paper can be used for the blade structural load measurement effectively.

Data Availability

The test and flight data used to support the findings of this study are available from the corresponding author upon request.

Conflicts of Interest

The authors declare that there are have no conflicts of interest.

Acknowledgments

This work was supported by the General Armament Department of China for the development of helicopter (Grant no. [2019] 553).

References

[1] J. L. J. Pereira, M. B. Francisco, L. A. De Oliveira et al., "Multi-objective sensor placement optimization of helicopter rotor blade based on Feature Selection," *Mechanical Systems and Signal Processing*, vol. 180, Article ID 109466, 2022.

[2] J. Zhou, L. Dong, W. Yang, and W. Yang, "Experimental study on transfer functions of an active rotor under different flight conditions," *Chinese Journal of Aeronautics*, vol. 35, no. 8, pp. 107–120, 2022.

[3] J. Zheng, "A flight load test method for helicopter rotor blade," *International Journal of Mechanical Engineering and Applications*, vol. 9, no. 5, 2021.

[4] Y. Dai, L. Wang, C. Yang, X. Zhang, C. Yang, and X. Zhang, "Dynamic Dynamic Gust Load Analysis for Rotorsust load analysis for rotors," *Shock and Vibration Vibration*, vol. 2016, Article ID 5727028, 12 pages, 2016.

[5] P. J. D. Alexander William, "Measurement and evaluation of helicopter flight loads spectra data," *Journal of the American Helicopter Society*, vol. 15, no. 3, 1970.

[6] K. Hacen, Z. Amira, and E. Tahar, "Optical fiber sensors in border detection application: temperature, strain and pressure distinguished detection using fiber Bragg grating and fluorescence intensity ratio," *Optik*, vol. 229, 2021.

[7] C. Zhou, Z. Yao, Y. Hu, and Z. Hu, "Application scheme of fiber bragg grating sensor in prefabricated building," in *Proceedings of the 2020 5th International Conference on Minerals Source, Geotechnology and Civil Engineering(MSGCE 2020)*, pp. 1110–1116, Singapore, April, 2020.

[8] J. C. Ho, H. C. Yeo, and H. Yeo, "Assessment of comprehensive analysis predictions of helicopter rotor blade loads in forward flight," *Journal of Fluids and Structures*, vol. 68, pp. 194–223, 2017.

[9] K. Dmitry, K. Sergey, M. Sergey et al., "Application of fiber bragg gratings as a sensor of pulsed mechanical action," *Sensors*, vol. 22, no. 19, 2022.

[10] H. Liu, W. Ge, Q. Pan et al., "Characteristics and analysis of dynamic strain response on typical asphalt pavement using Fiber Bragg Grating sensing technology," *Construction and Building Materials*, vol. 310, Article ID 125242, 2021.

[11] R. M. Liu, D. K. Liang, A. Asundi, D.-K. Liang, and A. Anand, "Small diameter fiber Bragg gratings and applications," *Measurement*, vol. 46, no. 9, pp. 3440–3448, 2013.

[12] R. J. Sun, Z. Sun, D. DanHui, and L. M. Sun, "An integrated FBG sensing system for bridge health monitoring," *Sensors and Smart Structures Technologies for Civil, Mechanical, and Aerospace Systems*, vol. 6174, 2006.

[13] G. Frank, G. Raphaël, D. Chris, V. L. Thijs, I. Platt, and S. Jerry, "Advanced landing gear fiber Bragg grating sensing and monitoring system," *Advances in Structural Engineering*, vol. 25, no. 11, 2022.

[14] D. Michal, K. Artur, R. Piotr et al., "Application of operational load monitoring system for fatigue estimation of main landing gear attachment frame of an aircraft," *Journal of Materials*, vol. 14, no. 21, 2021.

[15] J. Zheng, "A test method for helicopter landing gear load," *International Journal of Mechanical Engineering and Applications*, vol. 9, no. 1, 2021.